

The imprint of the cosmic dark ages on the near-infrared background

Ruben Salvaterra^{1★} and Andrea Ferrara²

¹SISSA, Via Beirut 4, 34100, Trieste, Italy

²Osservatorio Astrofisico di Arcetri, L.go E. Fermi 5, 50125 Firenze, Italy

Accepted 2002 October 31. Received 2002 October 18; in original form 2002 August 20

ABSTRACT

The redshifted light of the first (Population III) stars might contribute substantially to the near-infrared background (NIRB). By fitting recent data with models including up-to-date Population III stellar spectra, we find that such stars can indeed account for the whole NIRB residual (i.e. after ‘normal’ galaxy contribution subtraction) if the high-redshift star formation efficiency is $f_{\star} = 10\text{--}50$ per cent, depending on the initial mass function (the top-heaviest requiring lowest efficiency) and on the unknown galaxy contribution in the L band (our models, however, suggest it to be negligible). Such an epoch of Population III star formation ends in all models by $z_{\text{end}} \approx 8.8$, with a hard limit $z_{\text{end}} < 9$ set by J -band observations. To prevent an associated intergalactic medium (IGM) overenrichment with heavy elements compared with observed levels in the IGM, pair-instability supernovae must be the dominant heavy element source. Alternative explanations must break the light–metal production link by advocating very massive stars $M > 260 M_{\odot}$, locking their nucleosynthetic products in the compact remnant or by postulating an extremely inhomogeneous metal enrichment of the Ly α forest. We discuss these possibilities in detail along with the uncertainties related to the adopted zodiacal light model.

Key words: black hole physics – galaxies: formation – intergalactic medium – cosmology: theory.

1 INTRODUCTION

The cosmic infrared background (CIRB) can set important constraints on the star formation history of the Universe (e.g. Hauser & Dwek 2001 and references therein). The CIRB consists of the cumulative radiation from all extragalactic sources. In the near-infrared (NIR) the CIRB is dominated by starlight, whereas in the mid- and far-infrared it results from dust emission.

Different authors had provided measures of the near-infrared background (NIRB) in the J , K and L bands using the data from the Diffuse Infrared Background Experiment (DIRBE) instrument on board the *Cosmic Background Explorer* (COBE) satellite. Recently, Matsumoto et al. (2000) have accurately measured the NIRB from 1.4 to 4 μm , using the data taken with the near-infrared spectrometer (NIRS). The largest uncertainty on the NIRB measurements is caused by the subtraction of the interplanetary dust (IPD) scattered sunlight. In spite of this difficulty some studies have concluded that normal galaxies cannot account for the whole observed NIRB (Totani et al. 2001).

Bond, Carr & Hogan (1986) pointed out that the first population of zero-metallicity stars, the so-called Population III (Pop III), might contribute to the cosmic background in the near-infrared. More recently, Santos, Bromm & Kamionkowski (2002) suggested

that a significant part of the unaccounted NIRB could come from Pop III stars. They considered a very top-heavy initial mass function (IMF), assuming that all stars have masses $\gtrsim 300 M_{\odot}$ as recent three-dimensional numerical simulations seem to suggest (Bromm, Coppi & Larson 1999, 2002; Abel, Bryan & Norman 2000). In this paper we improve on these earlier studies in many respects. First, we confront theoretical predictions with the recent Matsumoto et al. (2000) data, which provides a much tighter test and constraint. Secondly, we consider the effect of several IMFs. Thirdly, we use the new stellar spectra of Schaerer (2002) for zero-age main-sequence (ZAMS) metal-free stars, including the nebular continuous emission found to be very important for stars with strong ionizing fluxes.

We fit the estimate of the unaccounted NIRB finding limits on the star formation efficiency and on the redshift at which the formation of Pop III stars ends. We compare our results with high-redshift observations and draw some results on intergalactic medium (IGM) metal enrichment arising from Pop III supernovae (SN).

The paper is organized as follows. In Section 2 we describe the background intensity calculation, the stellar spectra used, and how we model the IGM. In Section 3 the available data in the NIR range are reviewed along with the number counts of normal galaxies from deep field surveys. We discuss the results of our analysis in Section 4; in Section 5 we present our conclusions.

We adopt the ‘concordance’ model values for the cosmological parameters: $h = 0.7$, $\Omega_M = 0.3$, $\Omega_{\Lambda} = 0.7$, $\Omega_b = 0.038$, $\sigma_8 = 0.9$ and

★E-mail: salvater@sissa.it

$\Gamma = 0.21$, where h is the dimensionless Hubble constant, $H_0 = 100 h$ km s⁻¹ Mpc⁻¹; Ω_M , Ω_Λ and Ω_b are the total matter, cosmological constant and baryon density in units of the critical density; σ_8 gives the normalization of the power spectrum on $8 h^{-1}$ Mpc scale and Γ is the shape of the power spectrum. We use the power spectrum for the fluctuations derived by Efstathiou, Bond & White (1992).

2 COSMIC INFRARED BACKGROUND

The mean specific intensity of the background $I(\nu_0, z_0)$, as seen at frequency ν_0 by an observer at redshift z_0 , is given by

$$I(\nu_0, z_0) = \frac{1}{4\pi} \int_{z_0}^{\infty} \epsilon(\nu, z) e^{-\tau_{\text{eff}}(\nu_0, z_0, z)} \frac{dl}{dz} dz \quad (1)$$

(Peebles 1993). Here $\epsilon(\nu, z)$ is the comoving specific emissivity, $\nu = \nu_0(1+z)/(1+z_0)$, $\tau_{\text{eff}}(\nu_0, z_0, z)$ is the effective optical depth at ν_0 of the IGM between redshift z_0 and z , and dl/dz is the proper line element

$$\frac{dl}{dz} = c[H_0(1+z)E(z)]^{-1},$$

where c is the speed of light and

$$E(z) = [\Omega_M(1+z)^3 + \Omega_\Lambda + (1 - \Omega_M - \Omega_\Lambda)(1+z)^2]^{1/2}. \quad (2)$$

2.1 The comoving specific emissivity

The gas initially virialized in the potential well of the parent dark matter halo, can subsequently fragment and ignite star formation only if the gas can cool efficiently and lose pressure support. For a plasma of primordial composition at temperature $T < 10^4$ K, the typical virial temperatures of the early bound structures, the only efficient coolant is molecular hydrogen. Thus, a minimum H₂ fraction is required for a gas cloud to be able to cool in a Hubble time. As the intergalactic relic H₂ abundance falls short of such a requirement by at least two orders of magnitude, the fate of a virialized lump depends crucially on its ability to rapidly increase its H₂ content during the collapse phase. Once a critical H₂ fractional abundance of $\sim 5 \times 10^{-4}$ is achieved in an object, the lump will cool, fragment and eventually form stars. This criterion is met only by larger haloes, so that for each virialization redshift there will exist a critical mass, $M_{\text{min}}(z)$, for which protogalaxies with total mass $M_h > M_{\text{min}}$ form stars and those with mass $M_h < M_{\text{min}}$ do not. We adopt here $M_{\text{min}}(z)$ as computed by Fuller & Couchman (2000).

In the absence of additional effects that could prevent or delay the collapse, we can associate with each dark matter halo with mass $M_h > M_{\text{min}}$ a corresponding stellar mass

$$M_\star = f_\star \frac{\Omega_b}{\Omega_M} M_h, \quad (3)$$

where f_\star is the fraction of baryons able to cool and form stars; we will refer to this quantity as the star formation efficiency. Thus, the stellar mass per unit comoving volume at redshift z contained in haloes with mass $M_h > M_{\text{min}}(z)$ is given by

$$\rho_\star(z) = \int_{M_{\text{min}}(z)}^{\infty} n(M_h, z) M_\star dM_h, \quad (4)$$

where $n(M_h, z)$ is the comoving number density of dark matter haloes of mass M_h at redshift z given by Press & Schechter (1974).

The comoving specific emissivity, in units of erg s⁻¹ Hz⁻¹ cm⁻³, is then

$$\epsilon(\nu, z) = l_\nu(z) \rho_\star(z), \quad (5)$$

where $l_\nu(z)$ is the specific luminosity of the population (in erg s⁻¹ Hz⁻¹ M_⊙⁻¹) at redshift z (see Section 2.4).

2.2 The intergalactic medium

Absorption arising from intergalactic gas located in discrete systems along the line of sight can seriously distort our view of objects at cosmological distances. At wavelengths shortward of Ly α ($\lambda < 1216$ Å) in the emitter rest frame, the source continuum intensity is attenuated by the combined blanketing of lines in the Lyman series, and strongly suppressed by the continuum absorption from neutral hydrogen shortward of the Lyman limit in the emitter rest frame. As pointed out by Haiman & Loeb (1999) no flux is transmitted at wavelengths $\lambda_0 < \lambda_\alpha(1+z_s)$ from sources at redshift $1+z_s > 32/27(1+z_i)$, where $z_i = 6.2$ (Gnedin 2001) is the currently favoured reionization redshift.

The effective optical depth τ_{eff} through the IGM is defined as $e^{-\tau_{\text{eff}}} = \langle e^{-\tau} \rangle$, where the mean is taken over all the lines of sight to the redshift of interest. For a Poisson distribution of absorbers (Madau 1991, 1992),

$$\tau_{\text{eff}}(\nu_0, z_0, z) = \int_{z_0}^z dz' \int_0^\infty dN_{\text{HI}} \zeta(N_{\text{HI}}, z') (1 - e^{-\tau}), \quad (6)$$

where $\zeta(N_{\text{HI}}, z') = d^2N/dN_{\text{HI}} dz'$ is the distribution of the absorbers as a function of redshift and neutral hydrogen column density, N_{HI} ; $\tau(\nu')$ is the optical depth of an individual cloud for ionizing radiation at frequency ν' .

For the Lyman- α forest, in the wavelength range $\lambda_\beta < \lambda_0/(1+z_{\text{em}}) < \lambda_\alpha$, where $\lambda_\alpha = 1216$ Å and $\lambda_\beta = 1026$ Å, we have (Madau 1995)

$$\tau_{\text{eff}} = 0.0036 \left(\frac{\lambda_0}{\lambda_\alpha} \right)^{3.46}.$$

When $\lambda_0/(1+z_{\text{em}}) < \lambda_\beta$, a significant contribution to the blanketing opacity comes from the higher-order lines of the Lyman series. In the wavelength range $\lambda_{i+1} < \lambda_0/(1+z) < \lambda_i$, the total effective line-blanketing optical depth can be written as the sum of the contributions from the $j \rightarrow 1$ transitions,

$$\tau_{\text{eff}} = \sum_{j=2,i} A_j \left(\frac{\lambda_0}{\lambda_j} \right)^{3.46}, \quad (7)$$

where λ_j and the corresponding values for A_j are given in Table 1.

Continuum absorption from neutral hydrogen along the line of sight affects photons observed at $\lambda_0/(1+z_{\text{em}}) < \lambda_L$, where $\lambda_L = 912$ Å is the Lyman limit. We have

$$\tau = N_{\text{HI}} \sigma, \quad (8)$$

where $\sigma(\lambda_0, z) \sim 6.3 \times 10^{-18} (\lambda_0/\lambda_L)^3 (1+z)^{-3}$ cm² (Osterbrock 1989) is the hydrogen photoionization cross-section, and $(1+z_c) = (\lambda_0/\lambda_L)$ for $\lambda_0 > \lambda_L$, whereas for $\lambda_0 < \lambda_L$, H I absorbs photons all the way down to $z_c = 0$.

Table 1. Coefficients A_j corresponding to λ_j in equation (7).

j	λ_j (Å)	A_j
2	1216	3.6×10^{-3}
3	1026	1.7×10^{-3}
4	973	1.2×10^{-3}
5	950	9.3×10^{-4}

Table 2. Best-fitting value (Model A1) for A , β and γ (Fardal et al. 1998) used in equation (9).

N_{HI}	A	β	γ
$<10^{14}$	1.45×10^{-1}	1.40	2.58
$10^{14}-10^{16}$	6.04×10^{-3}	1.86	2.58
$10^{16}-10^{19}$	2.58×10^{-2}	1.23	2.58
$10^{19}-10^{22}$	8.42×10^{-2}	1.16	1.30

For the redshift and column density distribution of absorption lines, the usual form can be adopted

$$\zeta(N_{\text{HI}}, z) = \left(\frac{A}{10^{17}} \right) \left(\frac{N_{\text{HI}}}{10^{17} \text{ cm}^{-2}} \right)^{-\beta} (1+z)^\gamma, \quad (9)$$

where the values of coefficients A , β and γ in different ranges in N_{HI} are given in Table 2, and are taken from Fardal, Giroux & Shull (1998).

2.3 Scattering of Ly α photons

Ly α line photons from first galaxies are absorbed by neutral hydrogen along the line of sight (Gunn & Peterson 1965). However, they are not destroyed but scatter and diffuse in frequency to the red of the Ly α resonance owing to the Hubble expansion of the surrounding H I. Eventually, when their net frequency shift is sufficiently large, they escape and travel freely toward the observer. The profile results in a strong, asymmetric Ly α emission line around 1225 Å with a scattering tail extending to long wavelengths.

The resulting scattered line profile, $\Phi(\nu, z)$, has been simulated by Loeb & Rybicki (1999). Here, we use the fitting analytical expression given by Santos et al. (2002)

$$\Phi(\nu, z) = \begin{cases} \nu_*(z) \nu^{-2} \exp\left(\frac{-\nu_*}{\nu}\right) & \text{if } \nu > 0 \\ 0 & \text{if } \nu \leq 0, \end{cases} \quad (10)$$

$$\nu_*(z) = 1.5 \times 10^{12} \text{ Hz} \left(\frac{\Omega_b h^2}{0.019} \right) \left(\frac{h}{0.7} \right)^{-1} \frac{(1+z)^3}{E(z)}, \quad (11)$$

where $E(z)$ is defined in equation (2). Note that we have allowed the IGM in the vicinity of the emitting galaxy to be overdense by a factor $\delta \approx 10$, to account for the high clustering of first sources.

2.4 Emission from a Pop III ‘stellar cluster’

We calculate the emission of a Pop III ‘stellar cluster’ according to the equation

$$l_\nu(z) = \int_{M_l}^{M_u} F(\nu, M, z) \phi(M) dM, \quad (12)$$

where $\phi(M)$ is the IMF normalized so that $\int_{M_l}^{M_u} \phi(M) dM = 1$; M_l and M_u are the lower and upper mass limits. The spectrum of a star of mass M at the rest-frame frequency ν and redshift z is given by

$$F(\nu, M, z) = l_\nu^{\text{star}}(M) + l_\nu^{\text{neb}}(M) + l_\nu^{\text{Ly}\alpha}(M, z), \quad (13)$$

where $l_\nu^{\text{star}}(M)$ is the spectrum of a Pop III star of mass M , l_ν^{neb} is the emission of the nebula surrounding the star and $l_\nu^{\text{Ly}\alpha}(z)$ is the emission arising from Ly α line photons from a source at redshift z scattered by the IGM (see Section 2.3).

As spectra of Pop III we adopt here those modelled by Schaerer (2002) who relaxed some assumptions made in previous works

(Tumlinson & Shull 2000; Tumlinson, Giroux & Shull 2001; Bromm, Kudritzki & Loeb 2001b). Schaerer (2002) presented realistic models for massive Pop III stars and stellar populations based on non-LTE atmospheres, recent stellar evolution tracks and up-to-date evolutionary synthesis models. Moreover, he included nebular continuous emission, which cannot be neglected for metal-poor objects with strong ionizing fluxes. This process increases the total continuum flux significantly at wavelengths redward of Lyman- α and leads in turn to reduced emission-line equivalent widths.

We thus add the contribution of the nebular emission ($n_e = 100 \text{ cm}^{-3}$ is assumed) as described in Schaerer (2002):

$$l_\nu^{\text{neb}} = \frac{\gamma_{\text{tot}}}{\alpha_B} (1 - f_{\text{esc}}) q(H) \quad (14)$$

(e.g. Osterbrock 1989), where α_B (in units of $\text{cm}^{-3} \text{ s}^{-1}$) is the Case B recombination coefficient for hydrogen and f_{esc} is the ionizing photon escape fraction out of the idealized region considered here (we assume $f_{\text{esc}} = 0$); $q(H) = Q(H)/M$, where $Q(H)$ is the ionizing photon rate (in units of s^{-1}) for H and is given for different stellar masses in table 3 of Schaerer (2002). The continuous emission coefficient γ_{tot} , including free-free and free-bound emission by H, neutral He and singly ionized He, as well as the two-photon continuum of hydrogen is given by

$$\gamma_{\text{tot}} = \gamma_{\text{HI}} + \gamma_{2q} + \gamma_{\text{HeI}} \frac{n(\text{He}^+)}{n(\text{H}^+)} + \gamma_{\text{HeII}} \frac{n(\text{He}^{++})}{n(\text{H}^+)}. \quad (15)$$

The continuous emission coefficients γ_i (in units of $\text{erg cm}^3 \text{ s}^{-1} \text{ Hz}^{-1}$) are taken from Aller (1987) for an electron temperature of 20 000 K. The spectrum of a 1000- M_\odot star (with and without the nebular emission) and of a 5- M_\odot star are plotted in Fig. 1.

Finally, the emission of Ly α line photons is given by

$$l_\nu^{\text{Ly}\alpha}(z) = c_{\text{Ly}\alpha} (1 - f_{\text{esc}}) q(H) \Phi(\nu_{\text{Ly}\alpha} - \nu, z), \quad (16)$$

where $c_{\text{Ly}\alpha} = 1.04 \times 10^{-11} \text{ erg}$ (Schaerer 2002). The line profile $\Phi(\nu)$ is given in equation (10).

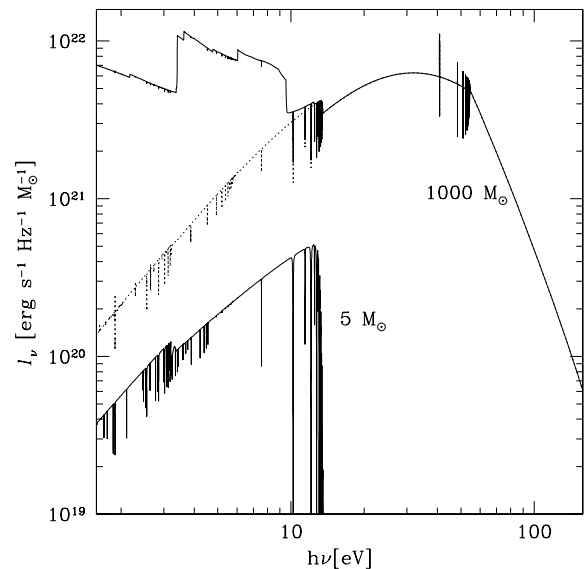


Figure 1. Spectra of individual Pop III stars plotted as the luminosity per unit of stellar mass (in $\text{erg s}^{-1} \text{ Hz}^{-1} M_\odot^{-1}$) versus energy (in eV). The spectrum of a 1000- M_\odot star with (solid line) and without (dashed) nebular emission and of a 5- M_\odot star are shown. For the 5- M_\odot star the contribution of the nebular emission is negligible.

2.4.1 Initial mass function

The issue of the mass distribution of the first metal-free stars has been tackled via various hydrodynamical models and other studies (e.g. Abel et al. 1998; Bromm et al. 1999, 2001a, 2002; Nakamura & Umemura 2001; Ripamonti et al. 2002). There seems to be an overall consensus that massive stars (up to $1000 M_{\odot}$) may form. Simulations seem to suggest that the primordial IMF might have been biased towards stellar masses $\geq 100 M_{\odot}$, but other studies (e.g. Nakamura & Umemura 2001) found that the formation of stars with masses down to $1 M_{\odot}$ is not excluded.

In the local universe the IMF is usually well described by the standard Salpeter law (Salpeter 1955)

$$\phi(M) \propto M^{-2.35}. \quad (17)$$

Larson (1998) suggested a different form for the high- z IMF. This has a universal Salpeter-like form at the upper end, but flattens below a characteristic mass, M_c , which may vary with time. By increasing M_c we can mimic a top-heavy IMF of Pop III stars,

$$\phi(M) \propto M^{-1} \left(1 + \frac{M}{M_c}\right)^{-1.35}. \quad (18)$$

Hernandez & Ferrara (2001) have explored the predictions of the standard hierarchical clustering scenario of galaxy formation, regarding the numbers and metallicities of Pop III stars that are likely to be found within our Galaxy today. By comparing these values with observational data, they suggested that the IMF of first stars was increasingly high-mass weighted towards high redshifts, levelling off at $z \geq 9$ at a characteristic stellar mass scale of $10\text{--}15 M_{\odot}$.

In view of our poor knowledge of the IMF at high redshift we consider here three different distributions of mass for the first population of stars: Salpeter, Larson with $M_c = 15 M_{\odot}$ (heavy IMF), and Larson with $M_c = 100 M_{\odot}$ (very heavy IMF). For all IMFs, $M_l = 1$ and $M_u = 1000 M_{\odot}$. In Fig. 2 we show the resulting spectra of a Pop III cluster at redshift $z_s = 10$ for the three different IMFs assumed.

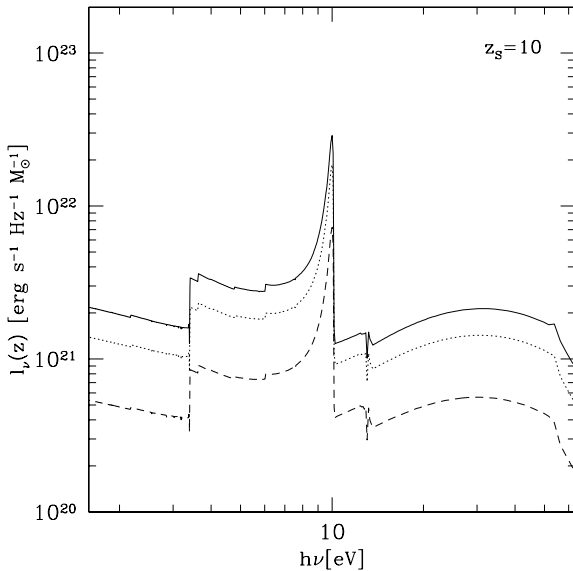


Figure 2. Pop III stellar cluster spectra for different IMFs. Dashed line, Salpeter; dotted line, heavy IMF; solid line, very heavy IMF. The sharp peak around 1220 \AA results from $\text{Ly}\alpha$ nebular emission for sources at $z_s = 10$, filtered through the IGM. The flux at $E > 13.6 \text{ eV}$ is then strongly suppressed by the absorption owing to the intergalactic gas (see Section 2.2).

3 OBSERVATIONAL CONSTRAINTS

Observations of the NIRB are seriously hampered by the strong atmospheric foreground (e.g. Mandolesi et al. 1998). On the other hand, space measurements are not easy because it is difficult to subtract correctly the contribution to the extragalactic background light by interplanetary dust scattered sunlight (zodiacal light). Using the data from the instrument DIRBE on board the *COBE* satellite and from the 2MASS data, Cambr sy et al. (2001) found a non-zero, isotropic background in the J and K bands. With the same data but a different zodiacal light model, Wright & Johnson (2001) extended the flux estimate to the L band. Cambr sy’s and Wright’s results in the J and K bands are compatible if the same zodiacal light model is applied. Matsumoto et al. (2000) provided a preliminary analysis of the NIRS data obtaining a detection of the NIRB in the $1.4\text{--}4 \mu\text{m}$ range. They applied the same zodiacal light model of Cambr sy et al. (2001) and obtained compatible results in the DIRBE bands. At 8000 \AA , Bernstein, Freedman & Madore (2002) observed a CIRB of $1.76 \pm 0.48 \times 10^{-5} \text{ erg s}^{-1} \text{ cm}^{-2} \text{ sr}^{-1}$, that is ~ 4 times smaller than the DIRBE and NIRS measurements in the J band, showing a break around $\sim 1 \mu\text{m}$. The integrated counts in the J and K bands from deep surveys do not account for the total NIRB (Madau & Pozzetti 2000; Totani et al. 2001). Totani et al. (2001) modelled the contribution of galaxies missed by deep galaxy surveys. They found it unlikely that the contribution of all the normal galaxies to the NIRB is larger than 30 per cent. All the available data are plotted in Fig. 3. In Table 3 the estimate of the NIRB from the DIRBE data (top panel) and the contribution of normal galaxies (bottom panel) are reported.

3.1 The DIRBE data

The Diffuse Infrared Background Experiment on board the *Cosmic Background Explorer* (see Boggess et al. 1992) satellite was

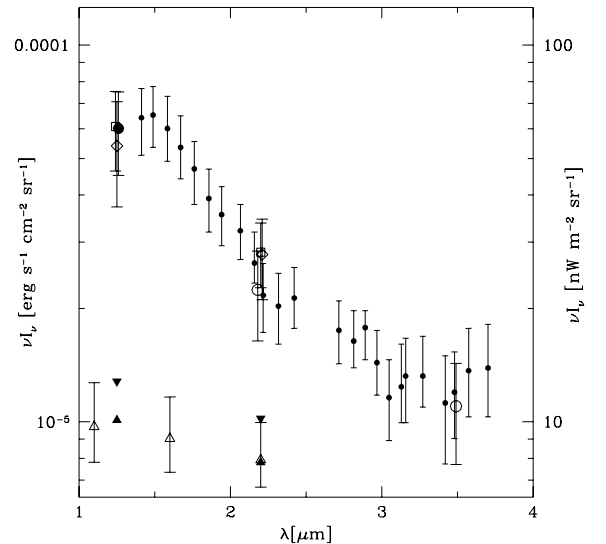


Figure 3. Available NIR data. The small filled circles are the NIRS data (Matsumoto et al. 2000). The open symbols are the DIRBE results: squares for Wright (2001), diamonds for Cambr sy et al. (2001) and circles for Gorjian et al. (2000). The big filled circle is the Kiso star count measurement. The data are slightly offset for clarity. The errors are at 1σ and for all the data the Kelsall et al. (1998) model for the zodiacal light is applied. The open triangles are the count integration from the *Hubble Deep Field* (Madau & Pozzetti 2000), whereas the filled triangles report upper and lower limits on the count integration from Subaru Deep Field when also the contribution of missed galaxies is considered (Totani et al. 2001).

Table 3. Summary of the recent observations of the NIRB from the DIRBE data (top panel). Units are $\text{nWm}^{-2} \text{sr}^{-1}$ (or $10^{-6} \text{erg s}^{-1} \text{cm}^2 \text{sr}^{-1}$). In the fourth column is given the model used to subtract the zodiacal light: ‘W’ stands for Wright (1998) and ‘K’ denotes Kelsall et al. (1998). In the bottom panel we show the results of count integration from the *Hubble Deep Field* (Madau & Pozzetti 2000) and from the Subaru Deep Field (Totani et al. 2001) surveys, the estimate of the contribution of missed galaxies (Totani et al. 2001. Model A: number evolution with $\eta \sim 1$; Model B: no number evolution with $\eta = 0$) and the total flux from all normal galaxies (Totani et al. 2001).

<i>J</i> band (1.25 μm)	<i>K</i> band (2.2 μm)	<i>L</i> band (3.5 μm)	M	Reference
	16.2 ± 6.4		W	Gorjian et al. (2000)
	22.4 ± 6.0	11.0 ± 3.3	K	
	(23.1 ± 5.9)	(12.4 ± 3.2)	W	Wright & Reese (2000)
(27.7 ± 14.5)	(19.9 ± 5.3)		W	Wright (2001)
60.8 ± 14.5	28.2 ± 5.5		K	
54.0 ± 16.8	27.8 ± 6.7		K	Cambrésy et al. (2001)
(24.3 ± 18)	(24 ± 6)	(13.8 ± 3.4)	W	Wright & Johnson (2001)
60.1 ± 15			K	Kiso star counts
Simple integration of observed galaxy counts				
$(9.7^{+3.0}_{-1.9})^a$	$7.9^{+2.0}_{-1.2}$			Madau & Pozzetti (2000)
10.9 ± 1.1	8.3 ± 0.8			Totani et al. (2001)
Estimated resolved fraction				
0.97	0.93			Model A
0.95	0.92			Model B
Contribution to the NIRB of all normal galaxy				
10.1–12.8	7.8–10.2			Totani et al. (2001)

^aEstimate at slightly different wavelengths.

designed to search for the cosmic infrared background from 1.25 to 240 μm . The DIRBE instrument (Silverberg et al. 1993) was an absolute photometer, which provided maps of the full sky in 10 broad-bands at 1.25, 2.2, 3.5, 4.9, 12, 25, 60, 100, 140 and 240 μm with a starlight rejection of $< 1 \text{ nW m}^{-2} \text{sr}^{-1}$ and an absolute brightness calibration uncertainty of 0.05 and 0.03 $\text{nW m}^{-2} \text{sr}^{-1}$, at 1.25 and 2.2 μm , respectively. A summary of the DIRBE results is provided by Hauser et al. (1998) and all the NIRB measures based on the DIRBE data are reported in Table 3 (top panel).

In the near-infrared bands the dominant foreground intensities in the DIRBE data are the zodiacal light and the light from stars in the Milky Way.

A first attempt to detect the NIRB from the DIRBE data was carried out by the DIRBE group but this gave only an upper limit and failed the tests of isotropy even in limited regions of the sky (Arendt et al. 1998). Dwek & Arendt (1998) made a correlation study for the *K* and *L* bands and obtained a lower limit for the *L* band.

Gorjian, Wright & Chary (2000) removed the foreground owing to Galactic stars by directly measuring all stars brighter than ninth magnitude at 2.2 and 3.5 μm in a $2 \times 2 \text{ deg}^2$ dark spot near the North Galactic Pole using ground-based telescopes. They calculated the contribution of fainter stars using the statistical model of Wainscoat et al. (1992) and subtracted the zodiacal light contribution using an improvement of the Wright (1998) model. Gorjian et al. found significant positive residuals in the *K* and *L* bands that they identified as a probable detection of the NIRB. Wright & Reese (2000) obtained a consistent estimate of the NIRB in the same bands using a different approach based on a histogram fitting method to remove the stellar foreground from the DIRBE data.

Wright (2001) used the Two Micron All-sky Survey (2MASS) data (Cutri et al. 2000) to remove the contribution of Galactic stars brighter than 14th magnitude from the DIRBE maps at 1.25 and 2.2 μm in four dark regions in the north and south Galactic Pole caps. For the subtraction of the zodiacal light foreground the model

presented in Gorjian et al. (2000) is applied. Cambrésy et al. (2001) have also used the 2MASS data to remove the Galactic stars from the DIRBE data, but they modelled the zodiacal light as in Kelsall et al. (1998). Their results agree with those of Wright (2001) if the same zodiacal light model is applied.

Recently, Wright & Johnson (2001) extended the analysis of Wright (2001) to 13 fields with a wide range of ecliptic latitudes tripling the number of pixels. They obtained an estimate of the NIRB at 1.25 and 2.2 μm consistent with the previous results. They also found a significant residual in the *L* band combining the Wright (2001) and Dwek & Arendt (1998) techniques, consistent with the result of Wright & Reese (2000).

Matsumoto et al. (in preparation) observed in the *J* band with the Kiso Schmidt Telescope toward the DIRBE dark spot. They subtracted all detected stars brighter than 14th magnitude and estimated the contribution of fainter stars using Cohen’s sky model (Cohen 1997). They used Kelsall’s zodiacal light model.

3.2 The NIRS data

The near-infrared spectrometer¹ is one of the focal instruments of the *InfraRed Telescope in Space* (IRTS) (Noda et al. 1994). The NIRS covers the wavelength range from 1.4 to 4.0 μm with a spectral resolution of 0.13 μm . The beam size is $8 \times 20 \text{ arcsec}^2$, which is considerably smaller than that of DIRBE; approximately 7 per cent of the sky is surveyed. In order to reduce the contribution from the faint stars, the sky at high latitudes ($b > 40^\circ$) is chosen.

Matsumoto et al. (2000) provided a preliminary analysis of the NIRS data, reporting detection of the cosmic infrared background based upon analysis of the 5 days of data that were least disturbed by atmospheric, lunar and nuclear radiation effects. The sky area analysed included Galactic latitudes from 40° to 58° , and ecliptic

¹<http://www.ir.isas.ac.jp/irts/nirs/index-e.html>

latitudes from 12° to 71° . NIRS is able to identify stars brighter than 10.5 mag at $2.24 \mu\text{m}$, whereas to find the contribution of fainter stars the Cohen model (1997) is used. The model of Kelsall et al. (1998) is applied to subtract the contribution of the zodiacal light foreground, interpolating between the DIRBE wavelengths to the wavelengths of the NIRS measurements. After subtraction of the IPD contribution, there remains a fairly isotropic residual emission, which they interpreted as evidence for a non-zero background. To obtain a quantitative value for the background at each wavelength they correlated their star-subtracted brightness at each point with the IPD model brightness, and used the extrapolation to zero IPD contribution as a measurement of the NIRB.

The NIRB intensities reported by Matsumoto et al. (2000) near 2.2 and $3.5 \mu\text{m}$ are similar to the values found by Gorjian et al. (2000). At shorter wavelengths, the NIRS results continue to rise steeply to $\sim 6.5 \times 10^{-5} \text{ erg s}^{-1} \text{ cm}^{-2} \text{ sr}^{-1}$ at $1.4 \mu\text{m}$. This is somewhat above the 95 per cent upper confidence limit at $1.25 \mu\text{m}$ of Wright (2001), but it is in agreement with the value obtained by Cambr esy et al. (2001) using the same zodiacal light model. The NIRS result implies an integrated background energy over the $1.4\text{--}4.0 \mu\text{m}$ range of $\sim 3.0 \times 10^{-5} \text{ erg s}^{-1} \text{ cm}^{-2} \text{ sr}^{-1}$.

The preliminary report by Matsumoto et al. (2000) does not provide details regarding systematic uncertainties in their results. The largest uncertainty in the reported NIRB values is attributed to the IPD model.

3.3 Galaxy contribution from deep counts

Deep optical and NIR galaxy counts provide an estimate of the extragalactic background light (EBL) coming from normal galaxies in the Universe. Madau & Pozzetti (2000) derived the contribution of known galaxies in the *UBVIJHK* bands from the *Southern Hubble Deep Field*. Although the slope of the number–magnitude relation of the faintest counts is flat enough for the count integration to converge, the recent observations of the NIRB (see the previous section) suggest that the diffuse EBL flux is considerably larger than the count integration. However, a considerable fraction of EBL from galaxies could still have been missed in deep galaxy surveys because of various selection effects.

Totani et al. (2001) using the Subaru Deep Field data (Maihara et al. 2001) have shown that more than 80–90 per cent of EBL from galaxies has been resolved in the *K* and *J* bands and that the contribution from missing galaxies cannot account for the discrepancy between the count integration and the NIRB observations. In Table 3 (bottom panel) we show the count integration in optical and NIR bands from Madau & Pozzetti (2000) and Totani et al. (2001), and the resolved fractions for two galaxy evolution models. The possible number evolution of galaxies is considered by a phenomenological model in which the Schechter parameters of the luminosity function have a redshift dependence of $\phi^* \propto (1+z)^\eta$ and $L^* \propto (1+z)^{-\eta}$; i.e. the luminosity density is conserved. In Model A an evolution with $\eta = 1$ is considered, whereas in Model B no evolution ($\eta = 0$) is assumed (see Totani et al. 2001 for more details). Currently, no measure of the contribution of normal galaxies to the NIRB in the *L* band is available the accurate measurement of which has to await for SIRTf.

4 MODEL VERSUS OBSERVATIONS

We compare the NIR data with the predictions of our model, summarized by equation (1). The data set is composed by the measurements of Matsumoto et al. (2000) and those obtained by the DIRBE data

using the Kelsall model for the zodiacal light emission as reported in Table 3 (top panel). For each wavelength we subtracted from the data the contribution of normal galaxies using the upper (lower) limits in the *J* and *K* bands, obtained by Totani et al. (2001) (last line of Table 3). As discussed already, for $\lambda > 2.2 \mu\text{m}$ no estimate of the NIRB arising from normal galaxies is available. Thus in the range $2.2\text{--}4 \mu\text{m}$ we consider two extreme cases: no contribution from normal galaxies (labelled with *cut*) and a constant contribution (labelled with *flat*).

4.1 Model results

The fitting results are quite sensitive to the adopted IMF and to the way we model the contribution of normal galaxies for $\lambda > 2.2 \mu\text{m}$. In Table 4 are reported the results of the fit for different IMFs, count integration model and z_{end} . The reported errors represent the statistical uncertainty of the fit, but systematic uncertainties that are difficult to evaluate might be present. In Fig. 4 we plot the values of the star formation efficiency and the corresponding χ^2/DOF (degree of freedom) as a function of z_{end} for the *cut* galaxy count model. The χ^2 increases rapidly as z_{end} becomes greater than 9, showing that in this case our model fails to account for the NIRB observation in the *J* band.

Table 4. Values of f_* from the fit to the data with different IMFs. The quoted statistical errors are at 95 per cent confidence limit.

IMF	Galaxy model	f_*		
		$z_{\text{end}} = 8$	$z_{\text{end}} = 9$	$z_{\text{end}} = 10$
Salpeter	Cut	0.37 ± 0.03	0.59 ± 0.05	0.89 ± 0.08
	Flat	0.24 ± 0.03	0.39 ± 0.05	0.58 ± 0.08
Heavy	Cut	0.15 ± 0.01	0.24 ± 0.02	0.36 ± 0.03
	Flat	0.10 ± 0.01	0.15 ± 0.02	0.23 ± 0.03
Very heavy	Cut	0.10 ± 0.01	0.15 ± 0.01	0.23 ± 0.02
	Flat	0.06 ± 0.01	0.10 ± 0.01	0.15 ± 0.02

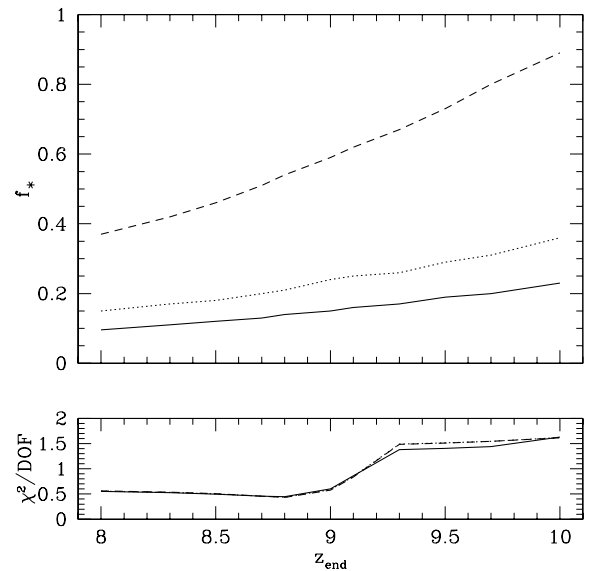


Figure 4. Star formation efficiency f_* accounting for the whole unexplained NIRB, as a function of redshift at which the formation of Pop III stars ends. The model *cut* for the counts integration for $\lambda > 2.2 \mu\text{m}$ is adopted. Dashed line: Salpeter IMF. Dotted line: heavy IMF. Solid line: very heavy IMF. The bottom panel shows the value of χ^2/DOF .

For a Salpeter IMF we find that a large fraction of baryons have to be turned into stars to account for the whole unexplained NIRB. This fraction goes from 37 per cent ($z_{\text{end}} = 8$) to 89 per cent ($z_{\text{end}} = 10$) if we consider the case of no contribution from normal galaxies for $\lambda > 2.2 \mu\text{m}$, which is slightly dependent on the choice of the upper and lower limits of the count integration. If we consider a constant (*flat* model) contribution of normal galaxies up to $2.2 \mu\text{m}$ the value of f_* goes from ~ 0.24 ($z_{\text{end}} = 8$) to ~ 0.58 ($z_{\text{end}} = 10$). The value of f_* decreases considerably if we consider a top-heavy IMF. For the *cut* model of the normal galaxy contribution, f_* ranges between ~ 0.15 ($z_{\text{end}} = 8$) and ~ 0.36 ($z_{\text{end}} = 10$) if $M_c = 15 M_\odot$ and between ~ 0.1 and ~ 0.23 if $M_c = 100 M_\odot$, whereas for the *flat* model we find f_* values from ~ 0.1 ($z_{\text{end}} = 8$) to ~ 0.23 ($z_{\text{end}} = 10$) with a heavy IMF and ~ 0.06 – 0.15 (for $z_{\text{end}} = 8$ – 10) with a very heavy IMF.

To find the best model, we allow both f_* and z_{end} to vary simultaneously and perform a two-parameter fit to the NIR data. The results are reported in Table 5. Again, the quoted errors take into account statistical uncertainties of the fit. In Fig. 5 we plot the best-fitting models for the *cut* contribution of normal galaxies. For the *flat* model the star formation efficiencies are significantly lower than in the *cut* case, but the χ^2/DOF always remains greater than 1.9,

Table 5. Best-fitting values for f_* and z_{end} with different IMFs. The quoted statistical errors are at 95 per cent confidence limit.

IMF	Galaxy model	f_*	z_{end}
Salpeter	Cut	0.53 ± 0.06	8.79 ± 0.10
	Flat	0.32 ± 0.04	8.69 ± 0.01
Heavy	Cut	0.21 ± 0.02	8.80 ± 0.01
	Flat	0.13 ± 0.02	8.75 ± 0.01
Very heavy	Cut	0.14 ± 0.01	8.83 ± 0.01
	Flat	0.09 ± 0.01	8.79 ± 0.01

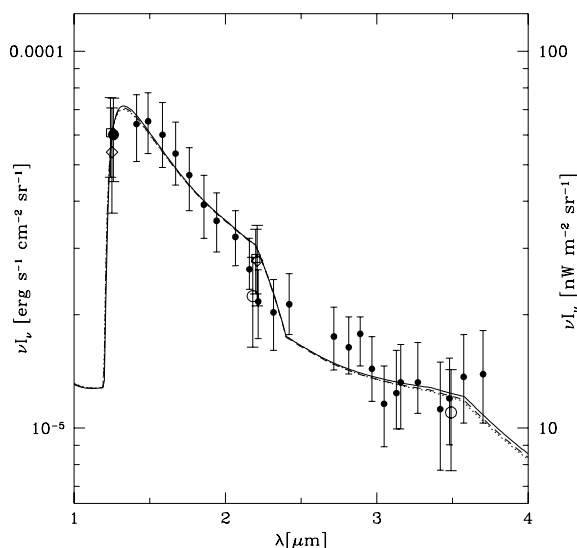


Figure 5. Best results of the fit for different IMFs. Dashed line, Salpeter IMF $z_{\text{end}} = 8.79$, $f_* = 0.53$; dotted line, heavy IMF $z_{\text{end}} = 8.8$, $f_* = 0.21$; solid line, very heavy IMF $z_{\text{end}} = 8.82$, $f_* = 0.14$. The model *cut* for the counts integration for $\lambda > 2.2 \mu\text{m}$ is adopted. The data are explained in Section 3 and in Fig. 3.

showing that a low contribution of normal galaxies for $\lambda > 2.2 \mu\text{m}$ is favoured by our model. A very remarkable result is the constancy of $z_{\text{end}} \approx 8.8$ in the various cases, independent of the IMF or the galaxy contribution model: its value is strongly constrained by the position of the break around $1 \mu\text{m}$. The break is principally owing to the Ly α line emission being redshifted into the *J* band, so that $\lambda_{\text{obs}} \sim \lambda_{\text{Ly}\alpha}/(1 + z_{\text{end}})$.

Barkana (2002) derived a value for f_* using the measured distribution of star formation rates in galaxies at various redshifts (Lanzetta et al. 2002) and semi-analytic models of hierarchical galaxy formation in a Λ CDM cosmology. He found a best-fitting value of $2.3^{+0.8}_{-0.5}$ per cent (2σ), neglecting dust obscuration, but the uncertainties on this evaluation are still large. If this value also applies to the first star formation, for a Salpeter IMF the Pop III contribution to the NIRB is not significant (< 10 per cent), whereas Pop III stars characterized by a top-heavy IMF continue to contribute substantially to the NIRB.

4.2 Associated metal enrichment

Recent theoretical analyses on the evolution of metal-free stars predict that the fate of the massive metal-free stars can be classified as follows (Heger, Woosley & Waters 2000; Chiosi 2000; Heger & Woosley 2002).

(i) $M > 260 M_\odot$: the nuclear energy release from the collapse of stars in this mass range is insufficient to reverse the implosion. The final result is a very massive black hole (VMBH) locking up all heavy elements produced.

(ii) $130 < M < 260 M_\odot$: the mass regime of the pair-instability supernovae ($\text{SN}_{\gamma\gamma}$). Pre-collapse winds and pulsations should result in little mass loss, the star implodes reaching a maximum temperature that depends on its mass and then explodes, leaving no remnant. The explosion expels metals into the surrounding ambient ISM.

(iii) $40 < M < 130 M_\odot$: black hole formation is the most likely outcome, because either a successful outgoing shock fails to occur or the shock is so weak that the fall-back converts the neutron star remnant into a black hole (Fryer 1999).

(iv) $8 < M < 40 M_\odot$: SN explosion from ‘normal’ progenitors.

Stars in the mass range (i) and (iii) above fail to eject most of (or all) their heavy elements, whereas type (ii) and (iv) stars eject metals into the IGM.

To estimate the metal production of Pop III objects we consider SN yields of Woosley & Weaver (1995) for progenitor metal-free stars between 8 and $40 M_\odot$ and the results of Heger & Woosley (2002) for very massive objects of pair-instability SNe originating from stars in the mass range ~ 130 – $260 M_\odot$. We neglect the contribution from long-lived intermediate-mass stars ($1 < M < 8 M_\odot$) as their evolution time-scale is longer than the Hubble time at the relevant redshift. The density of metals ejected into the IGM in units of the critical density, $\rho_c = 3H_0^2/8\pi G$, is obtained by

$$\Omega_Z(z) = f_Z(\phi)\Omega_*(z), \quad (19)$$

where f_Z is the fraction of metal ejected from normal and pair-instability supernovae; it depends on the adopted IMF, ϕ . Finally, $\Omega_*(z) = \rho_*/\rho_c$, where ρ_* is given in equation (4).

We calculate the IGM metallicity by imposing that the whole unaccounted NIRB is caused by Pop III stars. We use the best results for the efficiency reported in Fig. 5 for the *cut* model of the galaxy counts. We assume here that all the metal escapes into the IGM and that they are smoothly distributed. Fig. 6 shows the metallicity of the IGM (in solar units) as a function of redshift.

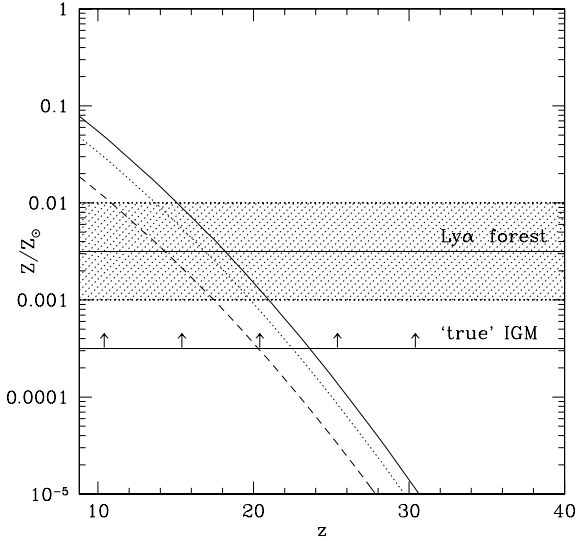


Figure 6. IGM metallicity as a function of redshift. Dashed line, Salpeter IMF; dotted line, heavy IMF; solid line, very heavy IMF. The curves are obtained by imposing that the whole unaccounted NIRB results from Pop III stars and the best results for star formation efficiency of Fig. 5 are assumed. The horizontal solid lines represent the value of the metallicity in the Ly α forest (Davé et al. 1998) and in the ‘true’ IGM (Songaila 2002).

We compare our results with the estimated value of metals in the Ly α forest ($10^{14.5} < N_{\text{HI}} < 10^{16.5} \text{ cm}^{-2}$) at $z \sim 3$ (Songaila & Cowie 1996; Davé et al. 1998) and in the ‘true’ IGM ($N_{\text{HI}} < 10^{14} \text{ cm}^{-2}$) at $z \sim 5$ (Songaila 2002). Identification of C IV, Si IV and O VI absorption lines that correspond to Ly α absorption lines in the spectra of high-redshift quasars has revealed that the low-density IGM has been enriched up to $Z_{\text{IGM}} \sim 10^{-2.5 \pm 0.5} Z_{\odot}$. For lower column density clouds (the ‘true’ IGM) Songaila (2002) found a lower limit on the IGM metallicity at $z \sim 5$ of $10^{-3.5} Z_{\odot}$.

With the assumed star formation efficiency ($f_{\star} = 0.534$ for a Salpeter; $f_{\star} = 0.214$ for a heavy IMF; $f_{\star} = 0.142$ for a very heavy IMF) the IGM would be enriched to the observed metallicity already at $z = 15\text{--}18$ for the Ly α forest value and at $z = 20\text{--}25$ for the ‘true’

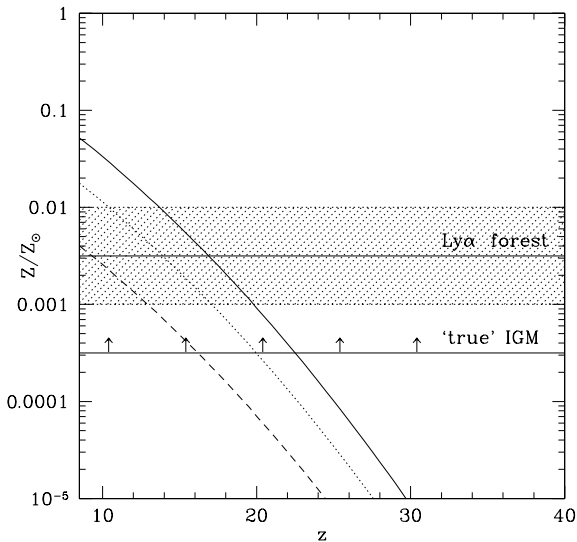


Figure 7. As for Fig. 6 but in the case in which only pair-instability SNe eject metals into the IGM. Dashed line, Salpeter IMF; dotted line, heavy IMF; solid line, very heavy IMF.

Table 6. The star formation efficiency and the fraction of NIRB from Pop III stars obtained by imposing that metals ejected by Pop III SNe do not exceed the mean observed values in the Ly α forest. The *cut* model for the galaxy counts is assumed.

IMF		f_{\star}	Percentage of NIRB
Salpeter	<i>All SN</i>	9.1×10^{-2}	17
	<i>Only SN$_{\gamma\gamma}$</i>	4.3×10^{-1}	80
Heavy	<i>All SN</i>	1.5×10^{-2}	7
	<i>Only SN$_{\gamma\gamma}$</i>	3.8×10^{-2}	18
Very heavy	<i>All SN</i>	0.6×10^{-2}	4
	<i>Only SN$_{\gamma\gamma}$</i>	0.8×10^{-2}	6

IGM lower limit (Fig. 6). As seen from Fig. 6, for $z \sim 8.8$ the mean IGM metallicity exceeds that observed in the Ly α forest by one order of magnitude.

As an alternative, we are thus forced to consider the analogous case in which only pair-instability SNe eject metals into the IGM (Fig. 7). For a Salpeter IMF the obtained metallicity is now consistent with the limits of the Ly α forest, whereas for a heavy IMF this value is slightly exceeded. For top heavy IMFs, for which the contribution of normal SNe is not so important, the results change only slightly.

In order to reduce these metallicity values further, we have to consider lower star formation efficiencies. Consequently, only a fraction of the NIRB can be Pop III stars. By imposing that Pop III stars do not eject more metals than the observed ones, we find self-consistent limits on the star formation efficiency and on the contribution of the first population of stars to the NIRB; Table 6 summarizes the results. Apart for the case of a Salpeter IMF in which only pair-instability SNe contribute to the metal enrichment of the IGM, the star formation efficiency has to be small ($\lesssim 10$ per cent) and the fraction of NIRB owing to Pop III stars is $\lesssim 20$ per cent.

The value obtained by Songaila (2002) for the ‘true’ IGM at $z \sim 5$ allows us to set a lower limit on the star formation efficiency and the contribution of Pop III stars to the NIRB. The efficiency has to be greater than a few $\times 10^{-4}$ to enrich the IGM to $Z \sim 10^{-3.5} Z_{\odot}$; thus, the Pop III star contribution to the NIRB is at least of the order of 0.4–1.7 per cent. This fraction increases up to 8 per cent if we consider the case in which only pair-instability SNe contribute to the metal enrichment of the universe.

5 DISCUSSION

Pop III stars can account for the entire NIRB excess if the high-redshift star formation efficiency is $f_{\star} = 10\text{--}50$ per cent, depending on the IMF and on the unknown ‘normal’ galaxy contribution in the L band. Our best results are obtained by considering a value of $z_{\text{end}} \approx 8.8$ for the redshift at which the formation of Pop III stars ends, almost independently of the IMF and of the ‘normal’ galaxy contribution model. A hard upper limit $z_{\text{end}} \leq 9$ is set by the J -band data. The above efficiency values are not at odds with expectations for objects forming in the dark ages (Madau, Ferrara & Rees 2001), although they seem to be higher than those found at lower redshifts.

In addition, the values of f_{\star} found should be considered as upper limits since the unaccounted NIRB level could be lower owing to a different zodiacal light subtraction. To quantify this uncertainty we have performed fits using the Wright zodiacal light model. In this case the DIRBE data alone are considered, as NIRS data are only available for the Kelsall model. We find that required star formation efficiencies decrease to 0.15–0.41 ($z_{\text{end}} = 8\text{--}10$) with a Salpeter IMF,

0.06–0.16 with a heavy IMF and 0.04–0.1 with a very heavy IMF; at $z_{\text{end}} = 8.8$ the resulting star formation efficiencies are 0.23 (Salpeter IMF), 0.09 (heavy IMF) and 0.06 (very heavy IMF). However, the errors are doubled with respect to the case of the Kelsall model for the zodiacal light emission. Also, the χ^2 analysis does not allow one to evaluate a unique redshift at which Pop III formation ends. This is a result of the fact that the break around 1 μm is not as sharp as in the previous case, as already mentioned.

As a consistency test, we have calculated the associated IGM metal enrichment. If the whole unaccounted NIRB is owing to Pop III stars, then we predict that the low-density ('true') IGM would be enriched at the observed mean value already by $z = 15$ –20, and that the Ly α forest data imply that either a Salpeter or a heavy IMF with characteristic mass $M_c = 15 M_\odot$ are acceptable, provided pair-instability SNe are the only source of heavy elements. This conclusion can be modified by the two following occurrences: (i) only stars with masses in excess of 260 M_\odot are formed, which lock their nucleosynthetic products into the VMBH remnant, effectively breaking the light–metal production link (Schneider et al. 2002) or (ii) metals are very inhomogeneously mixed in the IGM, with filling factors much smaller than unity (Scannapieco, Ferrara & Madau 2002) at these high redshifts. In both cases, the limits obtained from metallicity arguments are much weaker if not purely indicative.

To exemplify case (i), let us consider an IMF of the form $\phi(M) = \delta(1000 M_\odot)$. By imposing that the whole NIRB results from Pop III stars ($f_* = 0.04 \pm 0.01$ and $z_{\text{end}} = 8.83 \pm 0.01$) and assuming the *cut* model for the galaxy counts, we obtain a density of VMBH $\Omega_{\text{VMBH}}(z = 8.8) \sim 7 \times 10^{-4}$. This value is two orders of magnitude greater than the measured mass density in supermassive black holes (SMBHs) found from the demography of nuclei of nearby galaxies (Magorrian et al. 1998; Gebhardt et al. 2000), $\Omega_{\text{SMBH}} = 10^{-4} h \Omega_b = 2.66 \times 10^{-6}$ (Merritt & Ferrarese 2001), but it is unlikely that all VMBHs merge into SMBHs (Schneider et al. 2002; Volonteri, Haardt & Madau 2002). Hence it is not clear whether this scenario can represent a viable solution.

In the second case (ii), the measured metallicity might not be representative of the actual cosmic metal density and might result in a large overestimate of the amount of IGM heavy elements. In addition, note that the above estimates assume that all the produced heavy elements can escape into the IGM. If the metal escape fraction is equal to or less than ~ 10 per cent, the whole unaccounted NIRB could easily be caused by Pop III stars with no conflict with the observed IGM metallicity limits.

As a final remark, we point out that additional sources might contribute to the NIRB, as accretion on to black holes (Carr 1994) or decay of massive primordial particles (Bond et al. 1986).

ACKNOWLEDGMENTS

We thank D. Schaerer for providing Pop III spectra and V. Bromm and L. Danese for constructive and stimulating comments. This work was partially supported (AF) by the Research and Training Network 'The Physics of the Intergalactic Medium' set up by the European Community under the contract HPRN-CT2000-00126 RG29185.

REFERENCES

Abel T., Anninos P.A., Norman M.L., Zhang Y., 1998, *ApJ*, 508, 518
 Abel T., Bryan G.L., Norman M.L., 2000, *ApJ*, 540, 39
 Aller L.H., 1987, *Physics of Thermal Gaseous Nebulae*, Astrophysics and Space Science Library. Reidel, Boston

Arendt R.G. et al., 1998, *ApJ*, 508, 74
 Barkana R., 2002, *New Astron.*, 7, 337
 Bernstein R.A., Freedman W.L., Madore B.F., 2002, *ApJ*, 571, 56
 Boggess N.W. et al., 1992, *ApJ*, 397, 420
 Bond J.R., Carr B.J., Hogan C.J., 1986, *ApJ*, 306, 428
 Bromm V., Coppi P.S., Larson R.B., 1999, *ApJ*, 527, L5
 Bromm V., Ferrara A., Coppi P.S., Larson R.B., 2001a, *MNRAS*, 328, 969
 Bromm V., Kudritzki R.P., Loeb A., 2001b, 552, 464
 Bromm V., Coppi P.S., Larson R.B., 2002, *ApJ*, 564, 23
 Cambr esy L., Reach W.T., Beichman C.A., Jarrett T.H., 2001, *ApJ*, 555, 563
 Carr B.J., 1994, *ARA&A*, 32, 531
 Chiosi C., 2000, in Weiss A., Abel T., Hill V., eds, *The First Stars*. Springer-Verlag, Berlin, p. 95
 Cohen M., 1997, in Okura H., Matsumoto T., Roellig T.L., eds, *ASP Conf. Ser. Vol. 124, Diffuse Infrared Radiation and the IRST*. Astron. Soc. Pac., San Francisco, pp. 61–66
 Cutri R.M. et al., 2000, *Explanatory Supplement to the 2MASS Second Incremental Data Release*. <http://www.ipac.caltech.edu/2mass/releases/second/doc/explsus.html>
 Dav e R., Hellsten U., Hernquist L., Katz N., Weinberg D.H., 1998, *ApJ*, 509, 661
 Dwek E., Arendt R.G., 1998, *ApJ*, 508, L9
 Efstathiou G., Bond J.R., White S.D.M., 1992, *MNRAS*, 258, 1
 Fardal M.A., Giroux M.L., Shull J.M., 1998, *AJ*, 115, 2206
 Fryer C.L., 1999, *ApJ*, 522, 413
 Fuller T.M., Couchman H.M.P., 2000, *ApJ*, 544, 6
 Gebhardt K. et al., 2000, *ApJ*, 543, L5
 Gorjian V., Wright E.L., Chary R.R., 2000, *ApJ*, 536, 550
 Gnedin N.Y., 2001, *MNRAS*, submitted (astro-ph/0110290)
 Gunn J.E., Peterson B.A., 1965, *ApJ*, 142, 1633
 Haiman Z., Loeb A., 1999, *ApJ*, 519, 479
 Hauser M.G., Dwek E., 2001, *ARA&A*, 39, 249
 Hauser M.G. et al., 1998, *ApJ*, 508, 25
 Heger A., Woosley S.E., 2002, *ApJ*, 567, 532
 Heger A., Woosley S.L., Waters R., 2000, in Weiss A., Abel T., Hill V., eds, *The First Stars*. Springer-Verlag, Berlin, p. 121
 Hernandez X., Ferrara A., 2001, *MNRAS*, 324, 484
 Kelsall T. et al., 1998, *ApJ*, 508, 44
 Lanzetta K.M., Yahata N., Pascarella S., Chen H.-W., Fern andez-Soto A., 2002, *ApJ*, 570, 492
 Larson R.B., 1998, *MNRAS*, 301, 569
 Loeb A., Rybicki G.B., 1999, *ApJ*, 524, 527
 Madau P., 1991, *ApJ*, 376, L33
 Madau P., 1992, *ApJ*, 389, L1
 Madau P., 1995, *ApJ*, 441, 18
 Madau P., Pozzetti L., 2000, *MNRAS*, 312, L9
 Madau P., Ferrara A., Rees M., 2001, *ApJ*, 555, 92
 Magorrian J. et al., 1998, *AJ*, 115, 2285
 Maihara T. et al., 2001, *PASJ*, 53, 25
 Mandolesi N. et al., 1998, *A&A*, 331, 463
 Matsumoto T. et al., 2000, in Lemke D., Stickel M., Wilke K., eds, *ISO Surveys of a Dusty Universe, Lecture Notes in Physics Vol. 548*. Springer-Verlag, Berlin, pp. 96–105
 Merritt D., Ferrarese L., 2001, *MNRAS*, 320, L30
 Nakamura F., Umemura M., 2001, *ApJ*, 548, 19
 Noda M., Matsumoto T., Matsuura S., Noguchi K., Tanaka M., Lim M.A., Murakami H., 1994, *ApJ*, 428, 363
 Osterbrock D.E., 1989, *Astrophysics of Gaseous Nebulae and Active Galactic Nuclei*. University Science Books, Mill Valley
 Peebles P.J.E., 1993, *Principles of Physical Cosmology*. Princeton Univ. Press, Princeton
 Press W.H., Schechter P., 1974, *ApJ*, 187, 425
 Ripamonti E., Haardt F., Ferrara A., Colpi M., 2002, *MNRAS*, 334, 401
 Salpeter E.E., 1955, *ApJ*, 121, 161
 Santos M.R., Bromm V., Kamionkowski M., 2002, *MNRAS*, 336, 1082
 Scannapieco E., Ferrara A., Madau P., 2002, *ApJ*, 574, 590
 Schaerer D., 2002, *A&A*, 382, 28

- Schneider R., Ferrara A., Natarajan P., Omukai K., 2002, *ApJ*, 571, 30
Silverberg R.F. et al., 1993, in Scholl M.S., ed., *Infrared Spaceborne Remote Sensing*, Proc. SPIE Vol. 2019. SPIE, Bellingham, pp. 180–189
Songaila A., 2002, *ApJ*, 568, 139
Songaila A., Cowie L.L., 1996, *AJ*, 112, 335
Totani T., Yoshii Y., Iwamuro F., Maihara T., Motohara K., 2001, *ApJ*, 550, L137
Tumlinson J., Shull J.M., 2000, *ApJ*, 528, L65
Tumlinson J., Giroux M.L., Shull J.M., 2001, *ApJ*, 550, L1
Volonteri M., Haardt F., Madau P., 2002, *ApJ*, submitted (astro-ph/0207276)
Wainscoat R.J., Cohen M., Volk K., Walker H.J., Schwartz D.E., 1992, *ApJ Suppl.*, 83, 111
Woosley S.E., Weaver T.A., 1995, *ApJS*, 101, 181
Wright E.L., 1998, *ApJ*, 496, 1
Wright E.L., 2001, *ApJ*, 553, 538
Wright E.L., Johnson B.D., 2001, *ApJ*, submitted (astro-ph/0107205)
Wright E.L., Reese E.D., 2000, *ApJ*, 545, 43

This paper has been typeset from a $\text{\TeX}/\text{\LaTeX}$ file prepared by the author.